Luigi Carrino
Luigi Maria Galantucci
Luca Settineri   *Editors*

Selected Topics in Manufacturing

Emerging Trends from
the Perspective of AITeM's
Young Researchers

AITeM

Springer

Lecture Notes in Mechanical Engineering

Luigi Carrino · Luigi Maria Galantucci ·
Luca Settineri

Editors

Selected Topics in Manufacturing

Emerging Trends from the Perspective of AITeM's Young Researchers

Springer

Editors
Luigi Carrino
Dipartimento di Ingegneria Chimica, dei
Materiali e della Produzione Industriale
(DICMaPI)
University of Naples Federico II
Napoli, Italy

Luigi Maria Galantucci 🆔
Dipartimento di Meccanica Matematica e
Management (DMMM)
Politecnico di Bari
Bari, Italy

Luca Settineri 🆔
Dipartimento di Ingegneria Gestionale e
della Produzione (DIGEP)
Politecnico di Torino
Torino, Italy

About This Book

This book presents selected contributions on a wide range of scientific and technological areas covered by AITeM (the Italian Manufacturing Association).

First part *AITeM Young Researcher Award 2023* is written by young AITeM associates: the contributions reflect the multifaceted nature of the research in manufacturing, which takes advantage of emergent technologies and establishes interdisciplinary connections with various scientific and technological areas to move beyond simple product fabrication and develop a complex and highly interconnected value creation processes ecosystem pursuing high-value-added products to compete globally. It discusses the following topics: additive manufacturing, materials processing technology, assembly, disassembly and circular economy, manufacturing systems design and management, quality engineering and production metrology, process and system simulation, optimization and digital manufacturing.

An Editorial Committee composed by Luigi Maria Galantucci—Politecnico di Bari (President), Elena Bassoli—Università di Modena e Reggio Emilia, Luca Boccarusso-Università di Napoli Federico II, Davide Campanella—Università di Palermo, Gianni Campatelli—Università di Firenze, Antonio Del Prete—Università del Salento, Enrico Pisino—Competence Center +CIM 4.0 Torino, Loredana Santo—Università di Roma Tor Vergata, Enrico Savio—Università di Padova, Walter Terkaj—STIIMA CNR peer reviewed and selected ten contributions among 25 papers proposed for the Award.

Second part *White Papers* presents five contributions on some Emerging Trends in Manufacturing research. The contributions have been prepared by Working Groups that have formed around strategic research topics in the manufacturing sector, often related to emerging applications: the manufacturing of metallic prosthetic implants, the use of lasers in the production of products and components for electric mobility, digital twins applied to technologies and production systems, joining technologies in naval and marine applications, surface functionalization in biomedical implants. The papers here published aim to provide an overview of the new challenges posed by these frontier areas, demonstrating how only through the multidisciplinary and highly innovative approach that our community offers can these challenges be successfully addressed.

The White Papers underwent a reviewing process led by Prof. Luigi Carrino from the Università di Napoli Federico II to ensure their compliance with AITeM standards and to make their structure consistent.

Contents

AITeM Young Researcher Award 2023

3D Printing of Shape Memory Polymers: Embedding Nichrome-Wires to Enhance Their Performance

Gianni Stano, Antonio Pavone, and Gianluca Percoco

Abstract Shape memory polymers (SMPs) has recently gained popularity in the 3D printing field: the possibility to 3D print polymers capable to change their shape when triggered by a certain temperature, can lead to the fabrication of programmable structures. So far, the usage of solutions such as oven and warm water have been used to activate SMP, resulting in a lack of feasibility and difficult to be employed in real-life scenarios. In the present paper the authors propose a method to embed electrical nichrome-wires inside the 3D printed SMP during the fabrication process, in order to make the activation step easier, more feasible and faster. Several motions were reached when the 3D printed SMPs were activated, resulting appealing for the fabrication of soft robots. Moreover, complex structures made up of SMP material and flexible joint were also manufactured, proving that the proposed manufacturing method can be used to fabricate grippers and walking soft robots.

Keywords Shape memory polymers · 3D printing · Material extrusion · Soft robotics · Smart materials

1 Introduction

Over the years, Additive Manufacturing (AM) technologies have been largely employed for the fabrication of soft robots [1, 2] resulting in a reduction in costs, time and assembly tasks. From an actuation standpoint, 3D printed soft robots are based on pneumatic [3], electromagnetic [4], tendon driven [5], light [6], shape memory polymers (SMP) [7], shape memory alloys (SMA) [8], and hybrid systems [9]. The SMPs are a very promising class of actuators because of (i) lower cost, (ii) possibility to enable greater recovery deformation, (iii) biodegradability, and (iv) possibility to

G. Stano · A. Pavone (✉) · G. Percoco
Department of Mechanics, Mathematics and Management, Polytechnic of Bari, Via Orabona 4, 70125 Bari, Italy
e-mail: antonio.pavone@poliba.it

Interdisciplinary Additive Manufacturing (IAM) Lab, Polytechnic University of Bari, Viale del Turismo 8, 74100 Taranto, Italy

3

respond to more multiple stimuli [10] (even though one of the most studied domain is the temperature stimulus [11]). The SMP working mechanism is here described: its initial shape can be modified to a temporary shape, deforming the SMP at a fixed temperature above the glass transaction (Tg) temperature of the materials, named switching temperature (Ts). Cooling down the SMP, the temporary shape will be fixed: if the polymer is heated again above the Tg temperature, the SMP recover its initial shape [12, 13]. This particularly effect, called shape memory effect (SME) is a complex transformation that involves two class of SMP [14, 15]: (i) traditional one-way SMP (original shape-deforming shape-original shape), and (ii) two-way [16, 17] or more [18] SMP (original shape-deforming shape-original shape-deforming shape), able to remember two different shapes at low- and high-temperature.

On one hand SMPs do not required particular and complicated system to work such as cables, motors or pneumatic compressors, but on the other hand their activation is possible through external heat source [19] (often provided via oven and warm water) resulting in a lack of feasibility for real-life scenarios. A new challenge in soft robotics is the fabrication of SMP smart structures fabricated with embedded resistive wires, to improve SMPs usage [20, 21].

The low Tg (50–65 °C) of Polylactic Acid (PLA) makes it the most used thermo-plastic polymers to fabricate SMPs [12] in Fused Filament Fabrication (FFF) technology. In general, FFF printing parameters (infill and pattern) that affect recovery time and recovery rate of SMP structures has been largely studied [14, 22, 23]. Cesarano et al. [24] analyzed the SMP response at different time–temperature combinations and programming parameters. Ehrmann et al. [25] performed mechanical destructive tests and investigate the recovery rate of PLA sample changing infill patterns and percentage. Roudbarian et al. [26] improved the shape memory effect (SME) of PLA by following multi-layered and multi-material approaches. Yang et al. [27] improved physical properties of 3D-printed SMP parts by tuning appropriate process parameters.

Moreover, a new way to exploit the SME in FFF structures is the fabrication of structures composed of SMP parts and links made of non-shape memory material actuated with tendon driven [20]. An hybrid actuation system brings several benefits such as (i) increased bending performance, (ii) use of two materials with different stiffness degrees in the same printing cycle, and (iii) complex movements impossible to achieve using only one actuation system [28, 29].

In the present paper, a multi-material FFF approach has been used to create structures composed of two actuation systems in a single manufacturing cycle: SMP parts connected to soft parts (actuated using a tendon-driven system).

A novel method to enhance the additively manufactured SMP performance is also presented: resistive nichrome (NiCr) wires have been embedded inside the 3D printed SMP during the fabrication process (using the stop and go method), in order to make the SMA activation step easier, more feasible and faster. Several complex motions were obtained when the 3D printed structures (SMP and tendon driven) were activated, resulting appealing for the fabrication of soft robots mimicking animals, and showing that such complex motions are impossible to obtain using only one actuation system.

2   Shape Memory Polymers (SMPs) and Tendon Driven Characterization

The main idea of the present work is the one-shot fabrication of a complex, hybrid-actuated structure combining SMP and tendon driven system, in order to obtained bio-inspired motions [30]. To achieve this goal, a multi-material FFF machine, namely Ultimaker 5 (Ultimaker, The Netherlands) was used. the following parts have been fabricated in the same manufacturing cycle: (i) stiff parts made up with polylactic acid (PLA), with embedded NiCr wire coils (0.6 mm diameter, maximum temperature 1150 °C), (ii) flexible-soft joints made up with thermoplastic polyurethane (TPU). A 0.4 mm nylon tendon and a stepper motor were used to enabling the mechanical driven actuation.

2.1   Shape Memory Polymers: Stiff Parts

Before the fabrication of the complete structure, the SMP structure was studied to choose the best shape for the fabrication of the complex finger actuator. The stiff parts were printed using the process parameters listed in Table 1. In particular, as known from scientific literature [31], low values of printing speed and layer height (lh) increas the quality of the parts: in this work, the printing speed was set at 45 and 25 mm/s respectively for PLA and TPU, and the layer height at 0.1 mm. Moreover, the 45° raster orientation was used to overcome the sinking problem of the empty part (channels to embed resistive wires), and a maximum infill percentage of 100% was used to overcome the low heat diffusivity of the polymer.

PLA is characterized by a glass transaction temperature (Tg) between 55 and 65 °C (technical datasheet). Moreover, the start-and-stop (S&S) method [32] was used to embedded the NiCr wire inside the PLA parts: with a G-code modification it has been possible to pause the print, manually embed the wire and finally resume the manufacturing process to cover the NiCr wire, as shown in Fig. 1. The embedding of NiCr wire during the S&S is a manual process and strongly related to the operator skills, however it took the authors an average of 2 min to accomplish that.

Five different rectangular-sample (R0–) SMA structures, with embedded NiCr wires, have been designed and fabricated to evaluate the best shape in terms of

Table 1 Printing parameters

Printing parameters	PLA (Stiff parts)	TPU (Soft joints)
Printing speed (mm/s)	45	25
Infill percentage (%)	100–Lines	80–Lines
Raster angle (°)	45	45
Printing temperature (°C)	210	235
Layer height (mm)	0.1	0.1
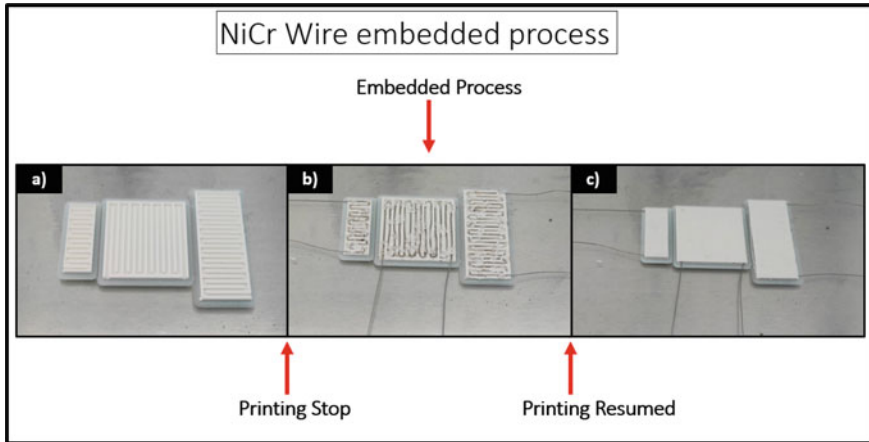
Fig. 1 A NiCr embedded process: **a** 3D printing process stopped when printing of sample channel is finished; **b** embedded NiCr resistance; **c** finale sample with embedded resistance after resumed printed

performance. The different SMP structures have been named R01, R02, R03, R04 and R05, respectively with x–y dimensions of 45×18 mm, 30×30 mm, 28×10 mm, 20×30 mm, 40×10 mm (see Fig. 2), keeping the thickness unchanged (fixed at 1.8 mm). The dimensions of the five different structures have been arbitrarily selected, in order to evaluate (i) the repeatability of the embedding process into different geometries, and (ii) how the dimensions of the structures affect their performance. Every version of the SMP-stiff part has been monolithically fabricated in a single-step printing cycle, resulting time and cost savings: for example, for R01 and R02 the time and cost are respectively 10 and 13 min, and 0.076 and 0.098 euro. It is worth mentioning that the spacing among the channel that housed the NiCr wire, has been set equal to 0.6 mm: this value was experimentally found as the minimum value ensuring a good 3D printing quality.

2.1.1 SMP-Stiff Part Compliance

For the characterization of the SMP-stiff part, the relationship between PLA compliance and local heating is studied. An ad hoc set-up was used to evaluate the compliance factor: (a) a power supply to heat up the embedded NiCr resistance, (b) a thermal imaging camera to evaluate the temperature of the NiCr wire, (c) weight of 50 and 75 g connected to the sample, and (d) a digital camera to take pictures at each increment of temperature to calculate the displacement.

The temperature of NiCr wire was incremented, starting from room temperature $T room$, to $T g$ and the compliance was calculated at 50, 55, 60 and 65 °C: a continuous current of $1.65A$ (tension of 6.30 V) was applied. Each R-sample was tested three times, calculating the standard deviation of the compliance factor for the different
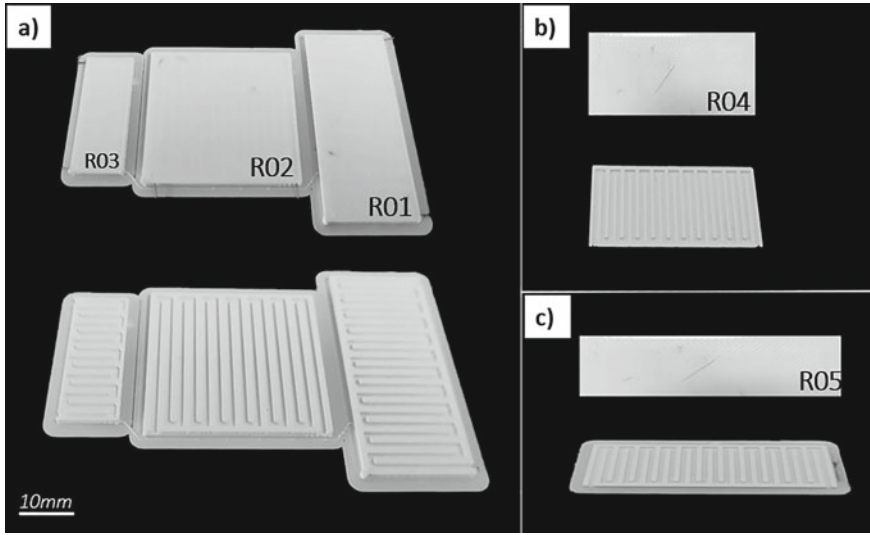
Fig. 2 Printed r-sample finished and internal channels

temperatures setting (see Table 2). Moreover, each sample was activated again to test the recovery shape, according to the SME. The compliance factor $C_m\left[\frac{mm}{N}\right]$ was calculated in according to [20].

$$C_m = \frac{1}{S} \tag{1}$$

where S is the stiffness of the part, calculated as the ration of the applied force $F[N]$ and the d, sample displacement [mm]:

$$S = \frac{F}{d} \tag{2}$$

Table 2 PLA stiff R-samples: compliance factor $\Delta C_m/C_{m0}$ versus temperature and load

T (°C)	$\Delta C_m/C_{m0}$ mean (Std. dev)					Load (g)
	R01	R02	R03	R04	R05	
50	2.97 (<0.001)	0.45 (<0.001)	0.43 (<0.001)	1.01 (<0.001)	4.92 (<0.001)	50
	2.31 (0.003)	1.39 (<0.001)	0.60 (0.05)	0.12 (<0.001)	2.68 (<0.001)	75
55	4.02 (<0.001)	1.89 (<0.001)	1.48 (<0.001)	1.22 (0.09)	5.67 (<0.001)	50
	2.92 (<0.001)	2.09 (0.02)	1.36 (<0.001)	1.29 (0.003)	4.40 (<0.001)	75
60	5.89 (0.02)	4.04 (0.02)	1.67 (0.002)	2.63 (0.15)	8.23(0.05)	50
	3.73 (<0.001)	3.43 (0.01)	2.40 (0.002)	3.17 (<0.001)	5.19 (<0.001)	75
65	7.75 (0.12)	6.81 (0.03)	2.24 (0.17)	3.32 (0.02)	9.04 (0.16)	50
	5.12 (0.002)	5.66 (0.02)	4.07 (0.01)	3.98 (0.03)	6.02 (0.06)	75

Starting from $Troom$, associated to C_{m0}, for each tested-temperatures the absolute compliance (ΔC_m) was calculated. R05 is the best in terms of compliance change, showing the maximum absolute compliance factor of 6.02 at $75g$ load and 65 °C. In Fig. 3 the absolute compliance for all the samples is shown.

Additionally, the testing phase has been used to obtain the behavior of the SMP samples at the fist activation (shape transforming phase) and at the second activation (shape recovery phase): such as the compliance testing, two loads (50 and 75 g), respectively generating two forces of $F1 = 0.49$ N and $F2 = 0.74$ N, were used. Firstly, for each rectangular sample, the internal NiCr resistance was heated from $Troom$ to T65 °C switching respectively from the rest position (initial) to final shape position, for each load. Secondly, each sample, after cooling, was re-heated from $Troom$ to T65 °C, respectively from shape position to recovery position (see Fig. 4). For the above-mentioned temperature values (50, 55, 60, and 65 °C) the displacement d was measured for each sample, during each test (see Table 2). $1.65 A$ of current was used. Moreover, the shaping and recovery time were measured to evaluate the actuation time for each sample (see Fig. 6). Particularly, as shown in Fig. 4e), the R05 sample confirms the compliance factor, resulting the only sample with a recovery position almost similar to the initial position. For example, the R05 changes its displacement from starting position to $d_{50g} = 31.12$ mm in 6 s and $d_{75g} = 36.52$ mm in 8 s respectively with 50 and 75 g load (see Fig. 4d). Finally, the R01 and R05 samples was tested in a vertical position to evaluate the bending angle with G-force application, as shown in Fig. 5.

As shown in Figs. 4 and 5, non-uniform deformation have been gotten: this might lead to unwanted failures during the exploitation of the SMP actuator. Due to the extremely huge design freedom offered from Additive Manufacturing (AM), new shapes can be easily fabricated to overcome this issue.

Concluding, R05 sample appears to be the best SMP-sample according to the performances shown. The R05 sample results the best in terms of (i) absolute compliance factor, (ii) SMP behavior with integration of NiCr wire for shape-recovery and (iii) low activation and recovery time. The impact of the manufacturing process on the performance shown by R05 have also been evaluated: five replications of R05 have been fabricated and tested. The standard deviation calculated while applying 75 g for the absolute compliance factor ΔC_m, activation time, and recovery time was respectively 0.7 (mean of 6.3), 1.3 (mean 7.2 s), and 2.1 (mean of 12.8 s). It stands out that the fabrication process is repeatable and has a very low impact on the performance shown from the SMP actuators. Also, from a geometric standpoint the R05 samples shows the highest ratio length/width (40 mm/10 mm): this might be related to the improved performances obtained, however more experiments are needed.

Also, a first attempt to characterize the fatigue life on R05 has been made: 10 consecutive activation cycles have been performed and the activation position, recovery position, activation time and recovery time were evaluated. In particular, all the four outputs shown a very low standard deviation (statistically not significant for every output), suggesting more cycles are needed to further study the fatigue behavior.
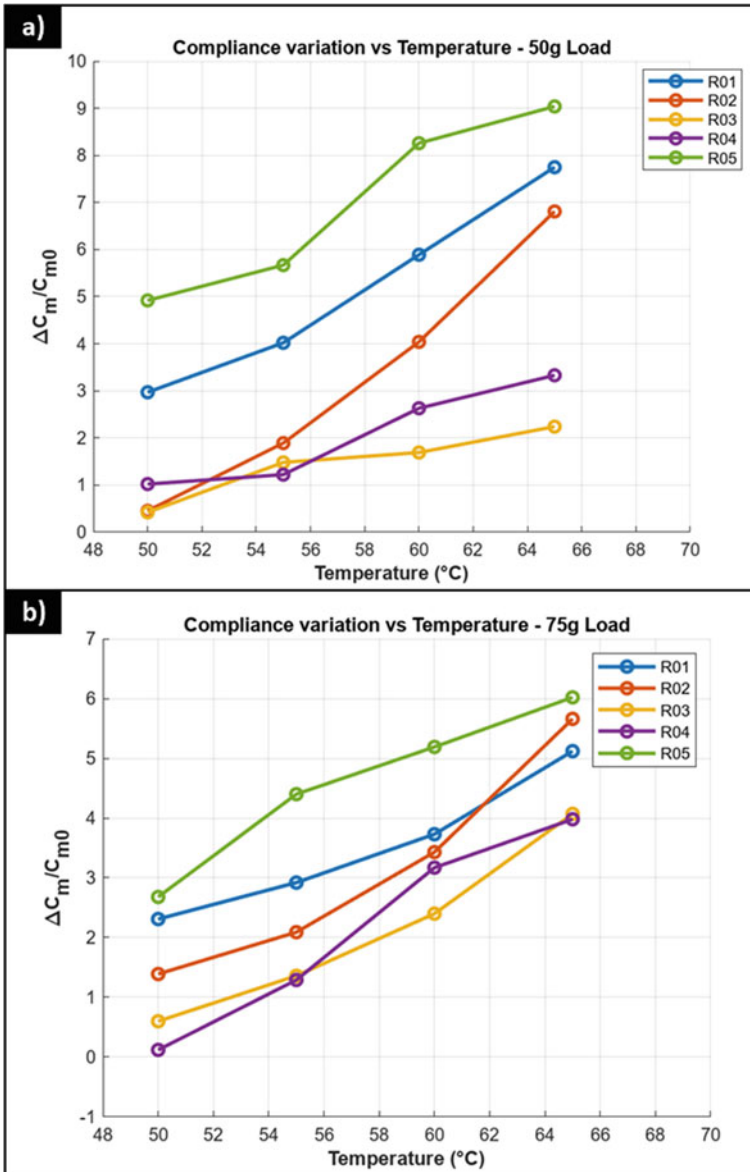
Fig. 3 Tested samples: **a** compliance variation with 50 g load application during temperature variation; **b** compliance variation with 75 g load application during temperature variation
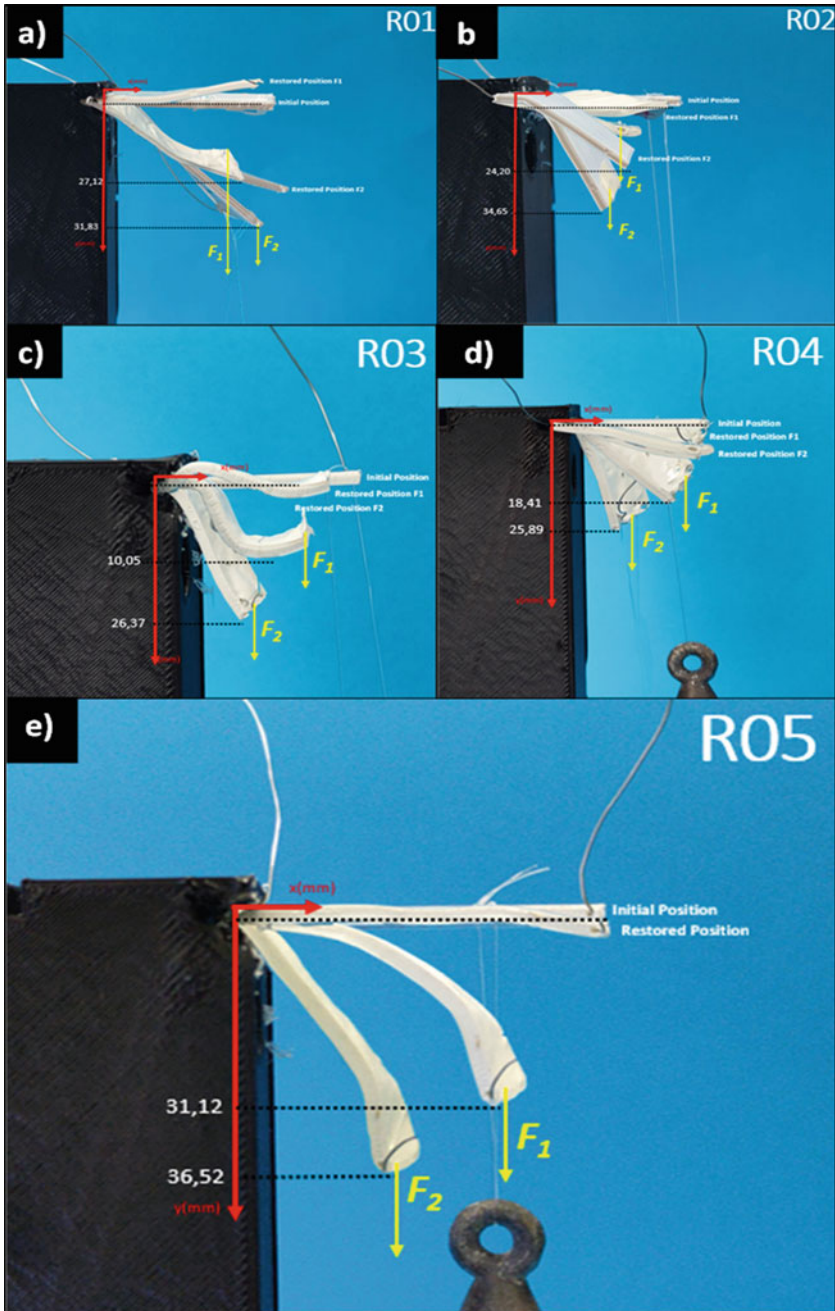
Fig. 4 Shape memory effect of tested samples comparing activation (using 50 and 75 g load) and recovery positions: **a** sample R01; **b** sample R02; **c** sample R03; **d** sample R04; **e** sample R05
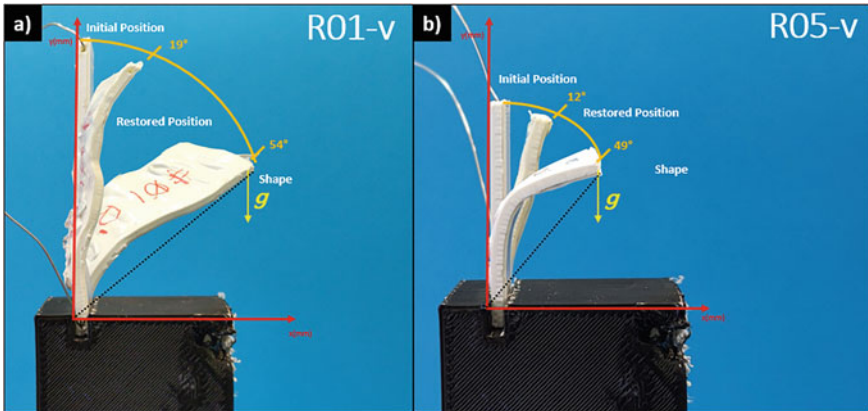
Fig. 5 Shape Memory Effect of tested vertical samples comparing activation (using 50 and 75 g load) and recovery positions: **a** sample R01; **b** sample R05

Since the R05 appear to be the most promising sample, two more variables such as Shape fixity and Shape recovery were evaluated based on 5 consecutive experiments performed on the same R05 sample: when applying 75 g as load, a mean shape fixity of 51° (standard deviation of 4.8°) and shepe recovery of 14° (standard deviation of 1.8°) was found. As shown in Fig. 5, the shape fixity and shape recovery values were calculated with respect to the origin.

2.2 Soft Joint: Tendon Driven Actuation

The SMP part, in the final version of the dual-mode actuator, is connected with a soft joint made up with TPU 95A, activated via a tendon-driven system (see Fig. 8a). In particular, mesh overlapping (mo), infill percentage (ip) and printing temperature of TPU were studied: three values of mesh overlapping were tested (0.15, 0.20, and 0.25 mm) combined to 50 and 80% of i p. In according to [33, 34], a T shape of the contact face between PLA and TPU was designed. After printing, the mesh overlapping and ip were tested with application of three different force of 5, 10, 20 N and 0.25 mm–80% were chosen for the following reasons:

- When a mesh overlapping of 0.15 mm (at 50 and 80% of in fill percentage) is set (Fig. 7a), the adhesion to PLA and TPU was not complete, and it led to the detachment of the joint during the force application
- Increasing the mesh overlapping to 0.20 and 0.25 mm, the adhesion between PLA and TPU increase, although the joint collapse in the range of 10–20 N when 50% of ip was set (see Fig. 7b)
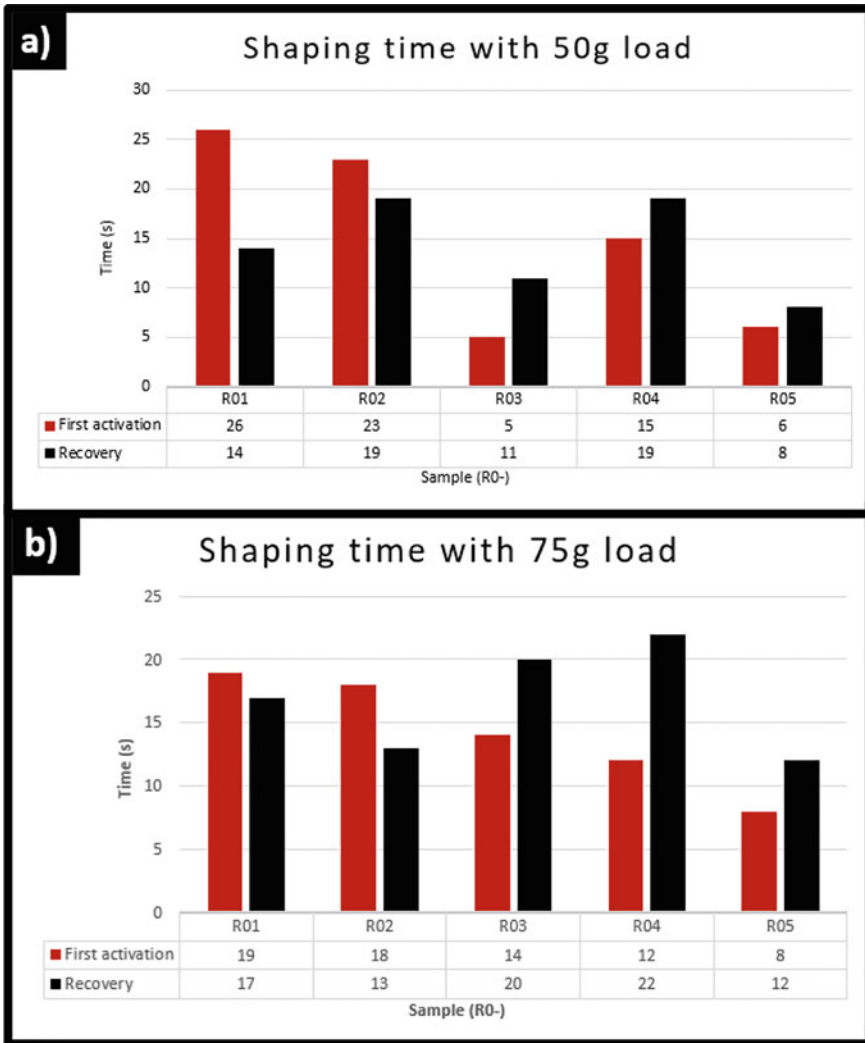
Fig. 6 Shaping time of R-sample during the first activation and during the second activation (recovery): **a** shaping time using 50 g load; **b** shaping time using 75 g load

- The 80% of infill percentage is a good compromise between the soft behaviour of the joint and the adhesion at the interface, setting 0.25 mm mesh overlapping (see Fig. 7c, d).

With a trial-and-error approach, the printing temperature of TPU was set at 240 °C to increase the adhesion to PLA: it is important to note that when temperature increase, proportional to mesh overlapping (set at 0.25 mm) and ip (set at 80%), the
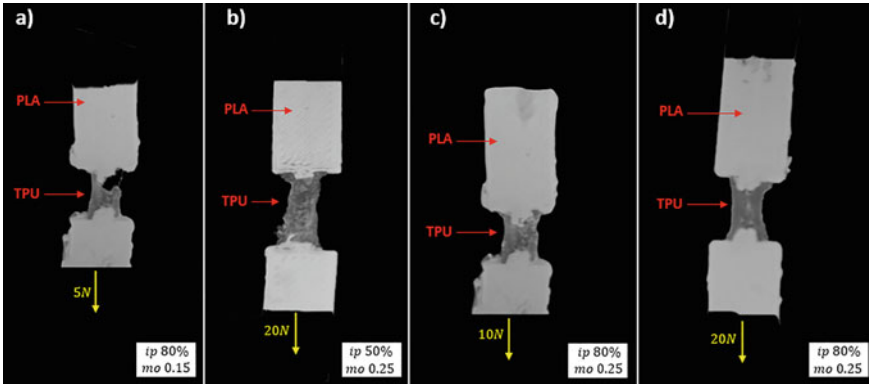
Fig. 7 Interface TPU-PLA tensile test: **a** collapsed joint with application of 5 N and mesh overlapping (mo) sets at 0.15 mm; **b** joint dilatation using 50% infill percentage (ip); **c** 10 N force application using 80% ip and 0.25 mm of mo; **d** 20 N force application
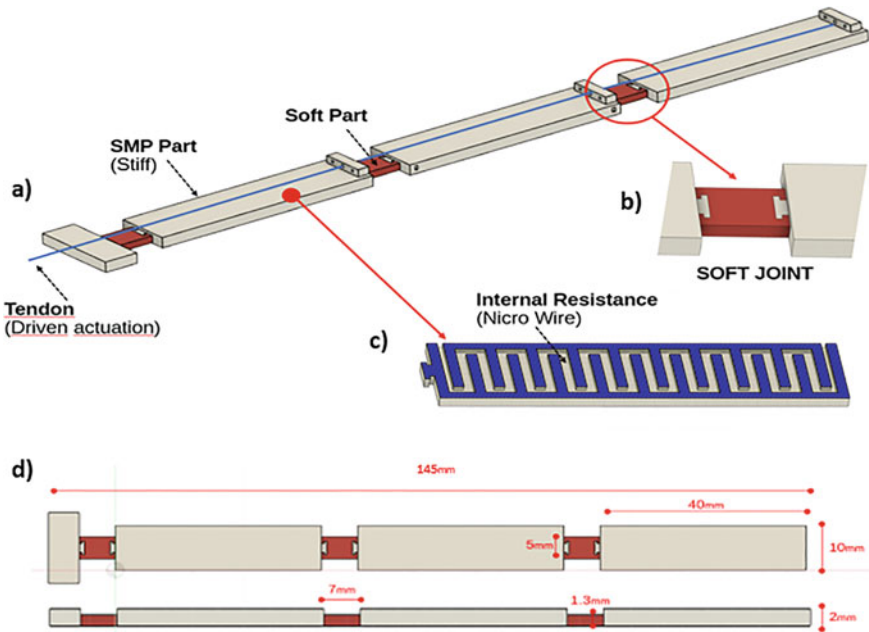
Fig. 8 Computer Aided Design (CAD) of complex finger structure: **a** representation of entirely structure; **b** interface between soft joint and stiff parts; **c** internal resistance channels; **d** dimension of the structure

joint became very functional and this parameters make the interface between PLA and TPU stronger.

3   Characterization of Dual-Activated (SMPs and Tendon-Driven) Structure

The proposed structure takes advantage of two actuation systems (SMP and tendon driven) resulting composed of PLA segments (SMP) and TPU segments (tendon driven) connected each others, as shown in Fig. 8.

The main reason leading to a dual actuation structure is the possibility to achieve complex motions (i.e. bending, twisting) impossible to achieve using a single actuation system. This structure is characterized by a manufacturing time and cost, respectively of 21 min and 0.89 Euro.

The fabricated finger was tested three times for each kind actuation system: (i) SMP actuation, (ii) tendon driven actuation and (iii) both actuation (combination of SMP actuation and tendon driven actuation). The tests were performed starting from resting condition (structure laying on the x-axis of Fig. 9): 1.68 A of current was provided to the NiCr wires to activate the SMP actuation, while a stepper motor was used to pull the tendon wire (tendon-driven actuation). When both the actuation systems were used at the same time, as shown in Fig. 9a), very complex motions were achieved: both bending and twisting were obtained. It is worth mentioning that no damages occurred after the three repetitions, however more tested have to be performed to quantify the fatigue behavior on soft robotics actuators.

It is necessary to note that the following limitations were present in this work:

- the number of the test on the complex actuator are not sufficiently to define a final behavior model, to estimate the right repetition of the movements.
- the tendon driven activation is faster than the SMP activation. An important part of future studies will be the reduction of the cooling time for the SMP by adding external cooling systems such as fan or cold water channels

4   Conclusions

In the present paper, a multi-material FFF approach was used for the monolithic fabrication of a structure able to perform several unconventional movements combining two different types of actuations: SMP system and tendon-driven system. The start and stop method has been successfully used to embed NiCr wires inside SMP structures making them more appealing for real-life scenarios overcoming the high activation time occurring when hot water or oven are used.

Fig. 9 Motions of complex finger structure, actuated using SMP actuation, Tendon driven actuation and both SMP and Tendon actuation: **a** real bending actuation; **b** software mapping

The present work lays the foundation (i) for an extensively usage of FFF technology to fabricate soft robots performing complex motions and (ii) for the fabrication of SMP-based structures with improved performance. Further investigation based on modelling the behavior of the proposed SMP actuators in relationship with the process parameters set in the slicing software will be performed.
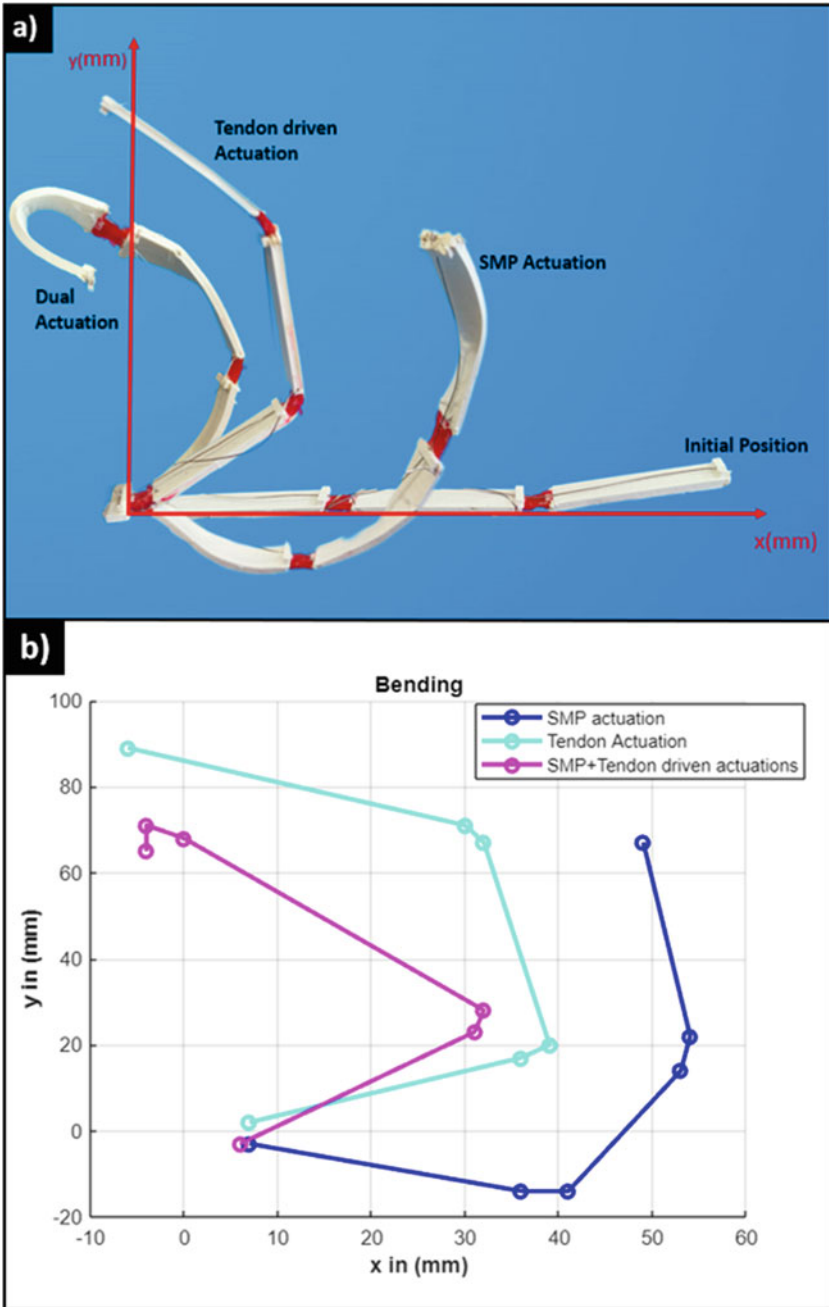
References

1. Stano G, Percoco G (2021) Additive manufacturing aimed to soft robots fabrication: a review. Extrem Mech Lett 42:101079. https://doi.org/10.1016/j.eml.2020.101079
2. Mitchell A, Lafont U, Hołyńska M, Semprimoschnig C (2018) Additive manufacturing—a review of 4D printing and future applications. Addit Manuf 24:606–626. https://doi.org/10.1016/j.addma.2018.10.038
3. Tawk C, Alici G (2021) A review of 3D-printable soft pneumatic actuators and sensors: research challenges and opportunities. Adv Intell Syst 3. https://doi.org/10.1002/aisy.202000223
4. Pavone A, Stano G, Percoco G (2023) One-shot 3D printed soft device actuated using metal-filled channels and sensed with embedded strain gauge, 3D print. Addit Manuf. https://doi.org/10.1089/3dp.2022.0263
5. Tawk C, Gillett A, Spinks GM, Alici G (2019) A 3D-printed omni-purpose soft gripper. 35(5):1268–1275
6. Huang C, Lv JA, Tian X, Wang Y, Yu Y, Liu J (2015) Miniaturized swimming soft robot with complex movement actuated and controlled by remote light signals. Sci Rep 5(July):1–8. https://doi.org/10.1038/srep17414
7. Chen T, Shea K (2018) An autonomous programmable actuator and shape reconfigurable structures using bistability and shape memory polymers, 3D print. Addit Manuf 5(2):91–101. https://doi.org/10.1089/3dp.2017.0118
8. Bodkhe S, Vigo L, Zhu S, Testoni O, Aegerter N, Ermanni P (2020) 3D printing to integrate actuators into composites. Addit Manuf 35:101290. https://doi.org/10.1016/j.addma.2020.101290
9. Aksoy B, Shea H (2022) Multistable shape programming of variable-stiffness electromagnetic devices. Sci Adv 8(21):1–14. https://doi.org/10.1126/sciadv.abk0543
10. Mehrpouya M, Vahabi H, Janbaz S, Darafsheh A, Mazur TR, Ramakrishna S (2021) 4D printing of shape memory polylactic acid (PLA). Polymer (Guildf) 230:124080. https://doi.org/10.1016/j.polymer.2021.124080
11. Ji Q, Wang XV, Wang L, Feng L (2022) Online reinforcement learning for the shape morphing adaptive control of 4D printed shape memory polymer. Control Eng Pract 126:105257. https://doi.org/10.1016/j.conengprac.2022.105257
12. Suethao S, Prasopdee T, Buaksuntear K, Shah DU, Smitthipong W (2022) Recent developments in shape memory elastomers for biotechnology applications. Polymers (Basel). 14(16). https://doi.org/10.3390/polym14163276
13. Koualiarella A et al (2020) Tuning of shape memory polymer properties by controlling 3D printing strategy. CIRP Ann 69(1):213–216. https://doi.org/10.1016/j.cirp.2020.04.070
14. Valvez S, Reis PNB, Susmel L, Berto F (2021) Fused filament fabrication-4d-printed shape memory polymers: a review. Polymers (Basel) 13(5):1–25. https://doi.org/10.3390/polym13050701
15. Leonés A, Sonseca A, López D, Fiori S, Peponi L (2019) Shape memory effect on electrospun PLA-based fibers tailoring their thermal response. Eur Polym J 117(May):217–226. https://doi.org/10.1016/j.eurpolymj.2019.05.014
16. Du L et al (2020) From a body temperature-triggered reversible shape-memory material to high-sensitive bionic soft actuators. Appl Mater Today 18:100463. https://doi.org/10.1016/j.apmt.2019.100463

17. Pandini S et al (2012) Two-way reversible shape memory behaviour of crosslinked poly(ε-caprolactone). Polymer (Guildf) 53(9):1915–1924. https://doi.org/10.1016/j.polymer.2012.02.053

18. Bai Y, Zhang X, Wang Q, Wang T (2014) A tough shape memory polymer with triple-shape memory and two-way shape memory properties. J Mater Chem A 2(13):4771–4778. https://doi.org/10.1039/C3TA15117D

19. Melly SK, Liu L, Liu Y, Leng J (2020) Active composites based on shape memory polymers: overview, fabrication methods, applications, and future prospects. J Mater Sci 55(25):10975–11051. https://doi.org/10.1007/s10853-020-04761-w

20. Stano G, Ovy SMAI, Edwards JR, Cianchetti M, Percoco G, Tadesse Y (2022) One-shot additive manufacturing of robotic finger with embedded sensing and actuation. Int J Adv Manuf Technol 467–485. https://doi.org/10.1007/s00170-022-10556-x

21. Takashima K, Sugitani K, Morimoto N, Sakaguchi S, Noritsugu T, Mukai T (2014) Pneumatic artificial rubber muscle using shape-memory polymer sheet with embedded electrical heating wire. Smart Mater Struct 23(12):125005. https://doi.org/10.1088/0964-1726/23/12/125005

22. Nam S, Pei E (2020) The influence of shape changing behaviors from 4D printing through material extrusion print patterns and infill densities. Materials (Basel) 13(17). https://doi.org/10.3390/MA13173754

23. Huang X, Panahi-Sarmad M, Dong K, Li R, Chen T, Xiao X (2021) Tracing evolutions in electro-activated shape memory polymer composites with 4D printing strategies: a systematic review. Compos Part A Appl Sci Manuf 147:106444. https://doi.org/10.1016/j.compositesa.2021.106444

24. Cesarano F, Maurizi M, Gao C, Berto F, Penta F, Bertolin C (2022) Science direct structural science direct science direct preliminary optimization of shape memory polymers geometric Preliminary optimization shape memory geometric parameters to enhance of the thermal loads' polymers activation range parameters loads' acti. Procedia Struct Integr 42(2019):1282–1290. https://doi.org/10.1016/j.prostr.2022.12.163

25. Ehrmann G, Ehrmann A (2021) Investigation of the shape-memory properties of 3D printed pla structures with different infills. Polymers (Basel) 13(1):1–11. https://doi.org/10.3390/polym13010164

26. Roudbarian N, Baniasadi M, Nayyeri P, Ansari M, Hedayati R, Baghani M (2021) Enhancing shape memory properties of multi-layered and multi-material polymer composites in 4D printing. Smart Mater Struct 30(10). https://doi.org/10.1088/1361-665X/ac1b3b

27. Yang Y, Chen Y, Wei Y, Li Y (2016) 3D printing of shape memory polymer for functional part fabrication. Int J Adv Manuf Technol 84(9–12):2079–2095. https://doi.org/10.1007/s00170-015-7843-2

28. Mao Y, Yu K, Isakov MS, Wu J, Dunn ML, Jerry Qi H (2015) Sequential self-folding structures by 3D printed digital shape memory polymers. Sci Rep 5:1–12. https://doi.org/10.1038/srep13616

29. Yamamura S, Iwase E (2021) Hybrid hinge structure with elastic hinge on self-folding of 4D printing using a fused deposition modeling 3D printer. Mater Des 203:109605. https://doi.org/10.1016/j.matdes.2021.109605

30. Kilbourne BM, Hutchinson JR (2019) Morphological diversification of biomechanical traits: mustelid locomotor specializations and the macroevolution of long bone cross-sectional morphology. BMC Evol Biol 19(1):1–16. https://doi.org/10.1186/s12862-019-1349-8

31. Dey A, Yodo N (2019) A systematic survey of FDM process parameter optimization and their influence on part characteristics. J Manuf Mater Process 3(3). https://doi.org/10.3390/jmmp3030064

32. MacDonald E, Wicker R (2016) Multiprocess 3D printing for increasing component functionality. Science (80) 353(6307):aaf2093. https://doi.org/10.1126/science.aaf2093

33. Dairabayeva D, Perveen A, Talamona D (2022) Investigation on the mechanical performance of mono-material versus multi-material interface geometries using fused filament fabrication. Rapid Prototyp J 29(11):40–52. https://doi.org/10.1108/RPJ-07-2022-0221
34. Stano G, Ovy SMAI, Percoco G, Zhang R, Lu H, Tadesse Y (2023) Additive manufacturing for bioinspired structures: experimental study to improve the multimaterial adhesion between soft and stiff materials, 3D print. Addit Manuf. https://doi.org/10.1089/3dp.2022.0186

Aerosol Jet Printing of 3D Biocompatible Gold Nanoparticle-Based Micro-Structures

Miriam Seiti, Paola Serena Ginestra, and Eleonora Ferraris

Abstract Aerosol Jet® Printing (AJ®P) is an additive manufacturing (AM) technique for the deposition of a functionalized jet on *free-form* substrates. AJ®P is mainly exploited for 2D printed electronics, nevertheless, is gaining attention in the bioelectronic field. Few emerging studies have also established AJ®P as a micro-AM 3D printing technique. In this context, the 3D AJ®P process has not been deeply analysed yet. This work proposes an unique study of novel 3D AJ® printed gold microstructures, as arrays of micropillars $\geq 40\,\mu$m, with aspect ratios ARs ≤ 9 and print times ≤ 10 min. Print parameters were investigated via a full factorial design against shape fidelity and resolution, using a layer-by-layer strategy. Specimens were thermally sintered, without any binding. Optical, electrical, and biocompatibility tests were conducted and a flexible 3D microelectrode array was printed as proof-of-concept. Future applications include in-vitro bioelectronics, thermoelectric, and batteries.

Keywords Additive manufacturing · Biomedical applications · Gold nanoparticle ink

1 Introduction

Since the late 1960s, micromanufacturing processes are being continuously investigated and improved for a variety of advanced applications, especially in the electronic, medical, automotive, and biotechnology industries [1]. Representative products of such technologies include (opto)micro-electromechanical systems (MEMS), micro-electronics, microfluidics, and bioelectronics.

M. Seiti (✉) · E. Ferraris
Department of Mechanical Engineering, Campus De Nayer, Leuven, KU, Belgium
e-mail: miriam.seiti@kuleuven.be

M. Seiti · P. S. Ginestra
Department of Mechanical Engineering, University of Brescia, Brescia, Italy

In this context, the development and exploitation of three-dimensional (3D) periodic microstructures with high aspect ratios (ARs) gained a considerable attention, especially for MEMS [2], micro-actuators [3], electrophysiological [4], microsensors [5], and scaffolds for cell guidance [6]. The major traditional microfabrication technologies refer to lithography-based processes (photolithography, molding, chemical etching, laser ablation, etc.) and micromachining processes (EDM, microextrusion, micro-injection molding, micro-embossing, etc.) [7]. In the last 40 years, Additive Manufacturing (AM) opened up even more possibilities for customized and versatile three-dimensional (3D) microstructures, especially with the use of stereolithography (SLA), fused filament fabrication (FFF), 3D Direct Writing (DW) techniques and hybrid technologies.

Particularly, 3D-DW techniques include droplet-, energy beam-, flow-, and tip-based (or nozzle) writing processes [8]. Among them, 3D-DW nozzle-based techniques (e.g. syringe- or jet-based printing) deal with viscoelastic inks which can be focalized or extruded through a deposition nozzle in a layer-by-layer (LBL) strategy for building up 3D complex and periodic structures at meso- and micro-scales [9]. A wide range of materials, among which metals, polymers, ceramics, and biological compounds, can be singularly or simultaneously printed for multifunctional devices.

Aerosol Jet® Printing (AJ®P) is an AM-DW nozzle-based technique which has been introduced in the market since the 1990s [10]. AJ®P has been conventionally used for the printed electronics (PE) industry, especially for the two-dimensional (2D) deposition of functional inks for passive and active elements on *free-form* substrates (3 or 5-axes platform) [11]. Examples of AJ® printed devices are flexible antennas [12], strain sensors [13], wearable devices [14], electrochemical sensors [15], batteries [16], and so on. The technology concerns the printing of inks in a liquid form which can be further aerosolized by means of a pneumatic or ultrasonic approach. Such inks can have a wide viscosity range of [1–1000] mPas, as long as their loading content has a particle size less than 500 μm. The final printed constructs can feature a size starting from 15 μm, with a minimum thickness of hundreds of nm. Moreover, differently from inkjet printing, AJ®P offers a variable stand-off distance, z [mm], from 1 to 5 mm. Because of such versatility, AJ®P has recently gained attention for life science, and tissue engineering (TE) applications [17–20]. AJ®P commercial inks are typically PE inks, including conductive metal- (such as silver nanoparticles-based, AgNPs inks) and polymer-based dispersions, or (UV curable) dielectrics. Most of those inks derive from inkjet dispersions which have been optimized to work with an AJ®P process. Although the portfolio of AJ®P inks is positively growing, few or even none of the commercial solutions can be currently applied for biomedical applications, especially if they are TE-oriented. Indeed, most of the traditional PE co-solvents applied in the ink formulation (such as xylenes, oils, and specific alcohols or glycols) generally induce a cytotoxic compounds in the cell culture, causing an unhealthy cellular state, which eventually leads to death. Therefore, novel biocompatible solutions have been proposed and successfully 2D AJ® printed, including natural (e.g. collagen [21], silk fibroin [22], gelatin [23]) or synthetic polymers (poly(3,4-ethylenedioxythiophene) polystyrene

sulfonate, PEDOT:PSS [17]), carbon-based (graphene, [24], carbon nanotubes [25], carbon ashes [25]), and also biological compounds (proteins [26]).

Very few among these inks can be exploited for bioelectrical interfaces, such as graphene and PEDOT:PSS-based solutions. Although their competitive cost, a trade-off between electronic/ionic conductivity and biocompatibility is inevitable when compared to precious noble metals, as gold or platinum. For instance, commercial gold nanoparticles (AuNPs)- or platinum nanoparticles (PtNPs)-based inks (mainly available for inkjet printing) have a conductivity 2 or 3 orders of magnitude higher than polymer-based inks. Their use is thus preferred for specific (bio)electronic applications which require high sensing performances and excellent oxidation stability, without compromising the biocompatibility. AuNPs-based inks are unique solutions with outstanding tunable properties (e.g., optical, thermal, electrical) and have been exploited for surface coating and PE, including electrochemical sensors [27], humidity sensors [28], and biosensors [29, 30]. The AuNPs composition can be adjusted for the desired application in terms of shape, size and surface chemistry [31] and the co-solvents can be selected to have low levels of cytotoxicity. In this way, they can be used also in TE, drug delivery and cancer therapy [32–34].

Since 2017, a couple of emerging studies demonstrated the capability to use the AJ®P technology for 3D micro-structuring and micro-fabrication (here referred as 3D AJ®P), including AgNPs-based lattices and micropillars arrays at ARs ~20 [35], AuNPs-based pillars at an AR ~3.5 [30], photo-reactive polymers-based pillars at ARs ≤ 11 [36], and PEDOT:PSS–CNTs-based micropillars at an AR ~3.3 [37]. However, these works lack of a thorough investigation of the effects of 3D AJ®P parameters on the printed microstructures, fundamental for evaluating the repeatability and process window.

Therefore, this manuscript aims to be among the first works that investigate and optimize the 3D AJ®P process via a design of experiment (DOE) approach for the 3D printing of periodic conductive microstructures (micropillars) against shape fidelity and reliability. A novel 3D AJ®P AuNPs-based ink is selected for the study, along with a validation of its conductivity and biocompatibility. Lastly, a flexible 3D microelectrode array chip is printed as proof-of-concept. Such 3D AuNPs-AJ® printed microstructures offer an exciting potential in a vast range of 3D electrical and bioelectrical applications, including energy harvesting devices, (bio)sensors, in-vitro electrophysiology and lab-on-chip devices.

2 Materials and Methods

The AJ®P process atomizes and deposits functional inks on *free-form* substrates, with a resolution scale up to 15 µm in line width and hundreds of nm in thickness [10]. In this study, the AJ®P ultrasonic configuration (U-AJ®P) will be investigated. Figure 1 reports the schematic visualisation of the 3D-AJ®P process, divided into its three main subprocesses: ink atomization and transport, collimation and in-flight jet, and aerosol impaction and impingement. In details, the selected ink is positioned into

an ultrasonic bath and it is sonically excited till the generation of atomized micro-droplets from its surface. The aerosolized mist is then transported via an inert gas (N_2) called carrier gas flow, $CGF = $ [0–50] sccm, into a transport tube. This tube is directly connected to the print head, in which a second inert gas (N_2), named sheath gas flow, $SGF = $ [0–200] sccm, aerodynamically focuses the mist into an aerosol jet. The jet exits the nozzle and the in-flight jet later impacts on the substrate at a decided stand-off distance, z [mm] of 3 mm, following a precise computer-aided design (CAD) file. A post-printing process is usually applied to sinter the printed metal-based structure. CGF and SGF are therefore considered two crucial parameters for the transport and in-flight of the aerosol jet. The ratio between SGF and CGF is known as focusing ratio $R_f = \frac{SGF}{CGF} \geq 1$, for a converged and focused aerosol jet which reduces undesired deposited satellite (or outlier) droplets at the edges of the printed patterns (known as overspray, OS). Moreover, high values of the platen temperature, T [°C] can allow a fast evaporation of the ink (co-)solvents, inducing a pre-sintering process for the building-up of 3D microstructures [39].
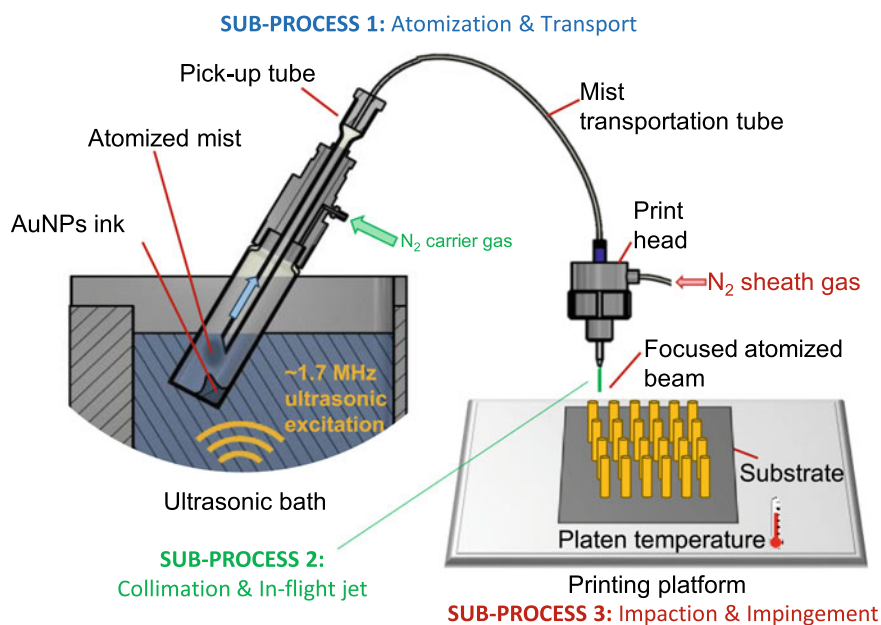

Fig. 1 Schematic figure of the 3D-AJ®P process, highlighting the three main sub-processes: (i) atomization and transport, (ii) collimation and in-flight jet, and (iii) impaction and impingement of the aerosol jet. Figure adapted from Degryse et al., International Conference on Biofabrication, 2021 [38]